Gas-Driven Ultrafast Reversible Switching of Super-hydrophobic Adhesion on Palladium-Coated Silicon Nanowires

*Jungmok Seo, Soonil Lee, Heetak Han, Hwae Bong Jung, Juree Hong, Giyoung Song, Suk Man Cho, Cheolmin Park, Wooyoung Lee, and Taeyoon Lee**

In nature, biological super-hydrophobic surfaces with a water contact angle (CA) greater than 150° exhibit two contrasting properties: water-repellent and water-adhesive. For example, the super-hydrophobic lotus leaves, and legs of water strides are highly water-repellent,[1–3] while the opposite can be observed in rose petals.[4] Such distinctive phenomena have received much attention in both academia and industry; super-hydrophobic surfaces with high water-repellant properties can be used for anti-fog windows,[5] anti-icing surfaces,[6] and fluid drag reduction.[7] On the other hand, water-adhesive super-hydrophobic surfaces were mainly used in advanced microfluidic applications, including no-loss water transporting systems,[8] and biochemical separation.[9] The adhesion properties of these super-hydrophobic surfaces were specifically controlled by tailoring the surface energy and nanoscale roughness of the surfaces.[10,11] However, most of the obtained super-hydrophobic surfaces exhibited either water-repellent or water-adhesive characteristics.[12,13] The reversible switching of super-hydrophobic adhesion properties within the same substrate, which requires elaborate regulation of surface roughness or surface energy, is greatly desired in advanced lab-on-a-chip platforms for biological or chemical detection where minimal liquid-substrate interaction is required.[14,15]

Despite large efforts to develop novel methods to manipulate the water-adhesive properties on a super-hydrophobic surface, only a few advances have been reported. Li et al.[16] first reported on the switching of super-hydrophobic adhesion properties on surfaces coated with side-chain liquid crystal polymer through thermally induced phase transition of the coated polymer layer, where a reversible change in the static and dynamic water CAs was achieved. However, the increase in the temperature may result in evaporation of the water droplet, and the process takes a long time owing to the slow cooling rate of the coated polymer layer. Several years later, they reported an in situ manipulation of water adhesion on the super-hydrophobic surface of a photo-sensitive polymer coating using ultraviolet irradiation to induce the polarity change, also resulting in a change of surface chemistry and roughness.[17,18] It has been demonstrated that the reversible switching of the water adhesion properties can be achieved within a minute.

Herein, we demonstrate a gas-driven ultrafast adhesion switching of water droplets on a dodecyltrichlorosilane (DTS)-coated super-hydrophobic surface of vertically aligned palladium (Pd)-coated Si (DTS Pd/Si) nanowire (NW) arrays. Si NW arrays aligned in the vertical direction were fabricated using the aqueous electroless etching (AEE) method, followed by DC magnetron sputtering of Pd, which resulted in the coating of Pd layers on the tip of the as-synthesized Si NW arrays. The water-repellant super-hydrophobic properties were obtained by simple dip-coating of DTS. Upon exposure to hydrogen gas, the prepared super-hydrophobic DTS Pd/Si NW arrays exhibited water-adhesive properties, which could be switched back to water-repellant properties in an ambient atmosphere. The reversible changes in the water-adhesive properties was almost instant, and was achieved through quick morphological phase transitions of the coated Pd layer in the DTS Pd/Si NW arrays induced by the adsorption and desorption of hydrogen (H) atoms while alternating the ambient conditions between a H_2 ambient and an atmospheric ambient. Potential applications of the suggested super-hydrophobic adhesion switchable surface were demonstrated, including the manipulation, transportation, and mixing of liquid droplets for advanced lab-on-a-chip devices.

Figure S1a and S1b in the Supporting Information show the typical cross-sectional and top-view SEM images, respectively, of the Pd/Si NW arrays with a deposited Pd thickness (t_{Pd}) of 15 nm. The fabricated Pd/Si NW arrays were vertically aligned over a large area with uniform lengths of ≈12 μm. The measured diameters of the Pd/Si NW arrays in a higher magnification image (not shown) ranged from 100 to 300 nm. As shown in Figure S1b in the Supporting Information, the Pd/Si NW arrays were bundled at their tips and formed locally clustered Pd/Si NW arrays, which can be attributed to the capillary force of the

Dr. J. Seo,[+] Dr. S. Lee,[+] Dr. H. Han, Dr. J. Hong, Prof. T. Lee
Nanobio Device Laboratory
School of Electrical and Electronic Engineering
Yonsei University
134 Shinchon-Dong, Seodaemun-Gu, Seoul 120-749
Republic of Korea
E-mail: taeyoon.lee@yonsei.ac.kr
Dr. H. B. Jung, Prof. W. Lee
Nano Device Laboratory
Department of Materials Science and Engineering
Yonsei University
262 Sengsanno, Seodaemun-gu, Seoul 120-749, Republic of Korea
Dr. G. Song, Dr. S. M. Cho, Prof. C. Park
Nanopolymers Laboratory
Department of Materials Science and Engineering
Yonsei University
262 Sengsanno, Seodaemun-gu, Seoul 120-749, Republic of Korea
[+]These authors equally contributed to this work.

DOI: 10.1002/adma.201300979

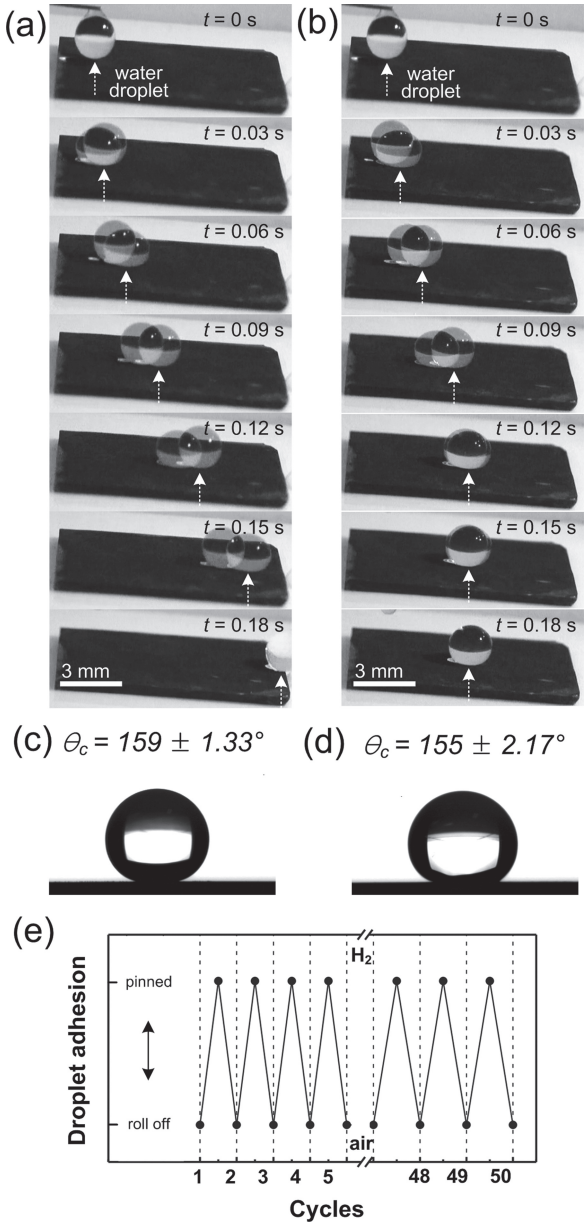

Figure 1. Sequential photographic images of an 8 μL water droplets on DTS Pd/Si NW arrays with t_{Pd} of 40 nm under: a) atmospheric ambient conditions, and b) 2% H_2 ambient, when the substrate was tilted by 5°. Optical images of an 8 μL water droplet on DTS Pd/Si NW arrays with t_{Pd} of 40 nm under: c) atmospheric ambient and d) 2% H_2 ambient. e) Reversible super-hydrophobic adhesion switching of the DTS Pd/Si NW arrays at repeated cycles (50 cycles) of alternating exposure to air and H_2 ambient.

liquid during the drying process of the Si NW arrays.[19,20] The measured distance between the adjacent Pd/Si NW clusters ranged from 1.3 to 3.7 μm, while the inter-distance between the individual Pd/Si NW arrays in a cluster was estimated to be in the range of sub-nm to a few nm. Due to the poor step coverage of the sputtering process, Pd atoms were hardly expected to reach down to the roots of the as-synthesized Si NW arrays, thus, most of the Pd layer was deposited at the tip of the as-synthesized Si NW arrays. It was observed that the surface profiles of Pd/Si NW arrays inherited the same surface morphology of as-fabricated Si NW arrays. The Pd/Si NW arrays were highly reproducible, with no significant variations in length, diameter and density.

To investigate the H_2 driven switching of super-hydrophobic adhesion on the vertically aligned DTS Pd/Si NW arrays, dynamic water droplet motions on the DTS Pd/Si NW arrays were captured under atmospheric H_2 ambients. During the experiment, the substrate was tilted with a very low angle of 5° and H_2 concentration was maintained at 2%. **Figure 1**a,b represent the time-sequential photograph images of a moving water droplet, of which the volume was controlled by a micro-needle to be approximately 8 μL, on a typical DTS Pd/Si NW array with t_{Pd} of 40 nm under atmospheric and H_2 ambient, respectively. In the images, the location of the moving water droplet is indicated by a white dotted-arrow. Under the atmospheric ambient (Figure 1a), the DTS Pd/Si NW arrays exhibited a highly water-repellent property. It was observed that the water droplets rolled off the surface along the direction of gravity as soon as they arrived on the surface of the DTS Pd/Si NW arrays, which was 0.03 seconds after the drop-casting. The measured velocity of the rolled off water droplet was 12.58 cm/s under the given tilt angle. On the other hand, after the exposure in H_2 ambient, the super-hydrophobic adhesion property of the DTS Pd/Si NW arrays was dramatically and immediately changed from water-repellent to water-adhesive (Figure 1b). The water droplets dropped on the DTS Pd/Si NW arrays were pinned on the substrate. When the H_2 exposed sample was re-exposed to air ambient, the super-hydrophobic adhesion property of the DTS/Si NW arrays was changed back to water-repellent within 3 seconds (see Supporting Information video for more details).

Figure 1c,d are typical photograph images of static water CA on the DTS Pd/Si NW arrays under atmospheric ambient and H_2 ambient, respectively. t_{Pd} was 40 nm and the water CAs of the DTS Pd/Si NW arrays were measured for more than five different locations and then averaged. The measured water CAs of the DTS Pd/Si NW arrays was 159 ± 1.33° under atmospheric ambient and slightly decreased to 155 ± 2.17° under 2% H_2 ambient. Thus, super-hydrophobic properties of the DTS Pd/Si NW arrays were confirmed under both conditions. The super-hydrophobicity of the DTS Pd/Si NW arrays could be explained by the Cassie-Baxter wetting state.[21] In this model, water CAs can be directly affected by the solid fraction of the surface (f), which is defined by the ratio of the actual area that can be contacted by the water droplet to the total surface area. The relationship between the water CA and the solid fraction in the Cassie-Baxter model can be expressed as follows:

$$\cos\theta_c = -1 + f(\cos\theta + 1), \quad (1)$$

where θ_c is the measured CA on a rough surface and θ is the intrinsic CA on a flat surface. The Cassie-Baxter model assumes that the water droplets are sitting on an "air pocket" between the water droplet and the top rough surface where water cannot not enter. When the water droplet was drop-cast on the surface of DTS Pd/Si NW arrays, trapped air pockets could be engendered between the water droplet and DTS Pd/Si NW arrays, resulting in a low f and large water CA. Figure 1e represents the reversible super-hydrophobic adhesion switching of the DTS

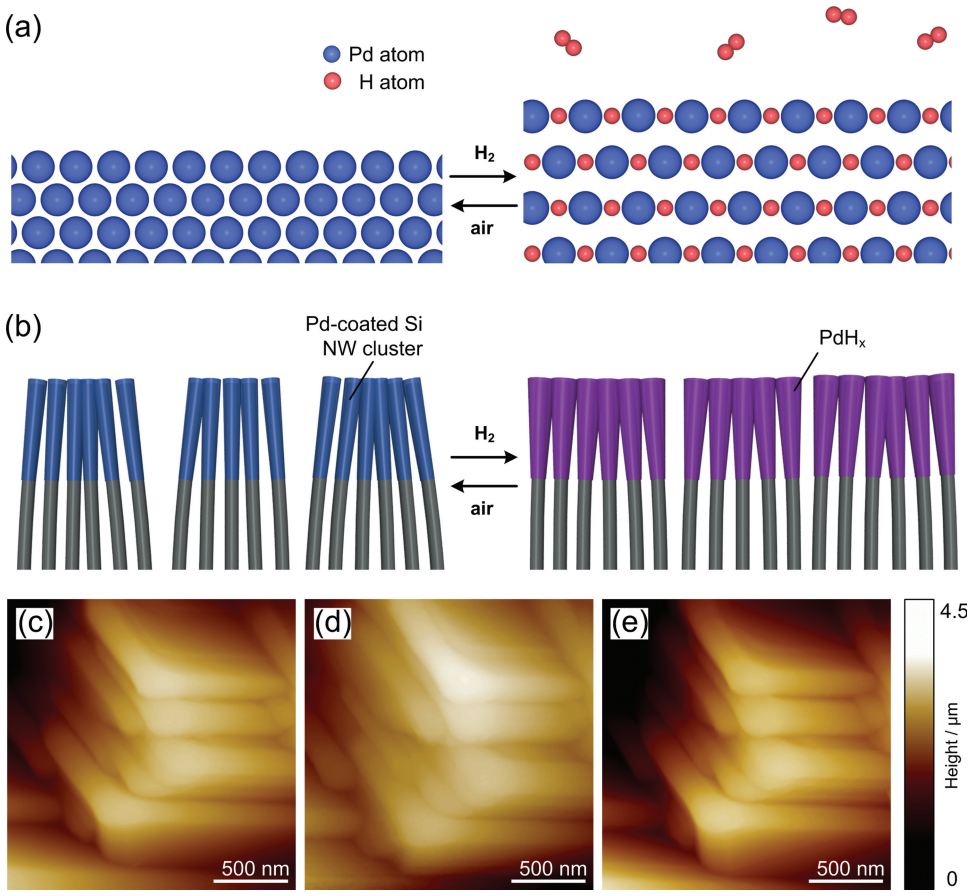

Figure 2. a) Schematic illustration of the H_2-induced volume expansion of Pd layer when the exposed to concentrated H_2 ambient. b) Schematic illustration of the volume expansion induced morphological changes of Pd/Si NW arrays. In situ AFM images of DTS Pd/Si NW arrays upon gas ambient conditions: c) as-prepared DTS Pd/Si NW arrays, d) 8% H_2 ambient exposed DTS Pd/Si NW arrays, and e) DTS Pd/Si NW arrays after being re-exposed in air ambient.

Pd/Si NW arrays at repeated cycles (50 cycles) of alternating exposure to air and H_2 ambient, showing sustainable reversible switching of water adhesion properties with high controllability.

The mechanism of the reversible switching of super-hydrophobic adhesion on the surface of DTS Pd/Si NW arrays could be explained by the H_2 gas-induced morphological changes of the coated Pd layer on the tips of the Si NW arrays, which results in an increase in pinning force between the Pd/Si NW clusters and the water droplet. **Figure 2**a depicts the schematic illustration showing the volume expansion of the coated Pd layer during exposure to H_2. The Pd atoms in the as-deposited Pd layer are in the form of a robust lattice structure, indicating that the crystal structure of the coated Pd layer is well organized. When exposed to concentrated H_2, H atoms are incorporated into the surface of the Pd layer with H_2 molecules breaking into single H atoms. The coated Pd layer is converted to PdH_x during exposure to H_2 ambient. At this stage, the Pd layer undergoes a phase transition from α- to β-phase. The Pd layer is expanded due to the filling of octahedral sites of the Pd system by H atoms, thereby causing a volumetric expansion of the Pd layer.[22] Notably, the DTS coating on the Pd layer does not significantly affect the hydrogen adsorption on the Pd layer, as evidenced from the previous study of hydrogen sensing devices.[23] After changing the ambient conditions from H_2 to atmosphere, the expanded Pd layer contracted to its initial volume, which is attributed to the fast reconversion of the PdH_x layer to Pd by desorption of H atoms under atmospheric conditions. Thus, this reversible volume change of the coated Pd layer led to surface morphology changes of DTS Pd/Si NW arrays, which could be strongly correlated to the pinning force of the water droplets. Figure 2b illustrates the volume expansion induced morphology changes of DTS Pd Si NW arrays. Under atmospheric conditions, the locally clustered vertical DTS Pd/Si NW arrays were separated by a few micrometers, as depicted in the left image of Figure 2b and confirmed from Figure S1b in the Supporting Information. Upon the flow of H_2 gas, the inter-distance between the clustered DTS Pd/Si NW arrays and individual DTS Pd/Si NWs was reduced, while the tips of the clusters, which were in direct contact with the water droplet, were enlarged due to the volumetric expansion of the coated Pd layer (right image of Figure 2b). Thus, the H_2-induced morphological changes of the DTS Pd/Si NW arrays resulted in increased contact line pinning force between the water droplet and the surface of DTS Pd/Si NW arrays. According to the previous report that investigated water droplet motions on nanopillar structures using the Cassie-Baxter model, the pinning force of

the water droplet on the nanostructured rough surfaces was dependent on the perimeter of the nanopillar structures.[24–27] Extrand[25] and Dorrer et al.[27] investigated the mechanism of water droplet movement on nanostructured surfaces and the causes of pinning force that resist the movement of water droplets. In the Cassie state built with periodic arrays of nanopillars, increasing the perimeter of the nanopillars resulted in a higher force to pin a contact line of the water droplet. In our report, the water droplet was in direct contact with the tips of the DTS Pd/Si NW clusters, and hence the enlarged size of the DTS Pd/Si NW clusters under a H_2 ambient could lead to an increased contact line pinning force, which could explain the gas-driven switching of the water-adhesive property of the super-hydrophobic DTS Pd/Si NW arrays.

To investigate the morphological changes of the DTS Pd/Si NW arrays by varying the gas ambient, in situ atomic force microscopy (AFM) characterization was carried out. Figure 2c–e represent the typical AFM images of DTS Pd/Si NW arrays upon alternating the ambient conditions between air and 8% H_2 ambient. The scanning size of all AFM images was 2 μm × 2 μm. As shown in Figure 2c,d, the size of the clustered DTS Pd/Si NW arrays enlarged when the substrate was exposed to the hydrogen ambient; the value of AFM root-mean-square (rms) roughness slightly increased from 400.1 to 442.1 nm, which was mainly due to the volumetric expansion of Pd layer. After re-storing the DTS Pd/Si NW arrays in air ambient, the DTS Pd/Si NW cluster was reverted to the initial state, and the measured AFM rmm roughness was also decreased to 404.3 nm. Consequently, the enlargement and shrinkage of Pd/Si NW clusters through alternating gas ambient could be attributed to the hydrogen induced volume change of the coated Pd layer on Si NW arrays, leading to the ultrafast super-hydrophobic adhesion switching of DTS Pd/Si NW arrays.

The super-hydrophobic adhesion force of water droplets on the DTS Pd/Si NW arrays is associated with the tip sizes of the clustered Pd-coated NWs, which are directly related to *f* of the DTS Pd/Si NW arrays. According to the thickness of Pd layer, *f* could be adjusted. To closely examine the relationship between the tip sizes of the DTS Pd/Si NW clusters and the water pinning force, we varied t_{pd} and observed the resulting changes in *f*. Figures S2a–c in the Supporting Information represent typical top-view SEM images of the DTS Pd/Si NW arrays where t_{pd} was: a) 10 nm, b) 40 nm, and c) 100 nm. The left column of the SEM images present top-views, and the right column that show the digitalized images of the corresponding SEM images. Digitalized images were obtained by first adjusting the brightness contrast balance to effectively identify the tips of the clustered DTS Pd/Si NW arrays which make direct contact with the water droplet, followed by changing the color contrast. *f* in contact with the water droplet was estimated by the ratio of the areas constituting the digitalized image with color to black areas. It was observed that the size of a single bundled DTS Pd/Si NW cluster was increased as thicker layers of Pd were deposited, consequently resulting in an increase in *f*. Figure S2d in the Supporting Information shows the changes in *f* of the DTS Pd/Si NW arrays with varying t_{pd} from 0 to 100 nm; with increasing t_{pd} from 0 to 100 nm, *f* was gradually increased from 0.11 to 0.21.

The pinning force of water droplets on the DTS Pd/Si NW arrays in our model system could be estimated using the water

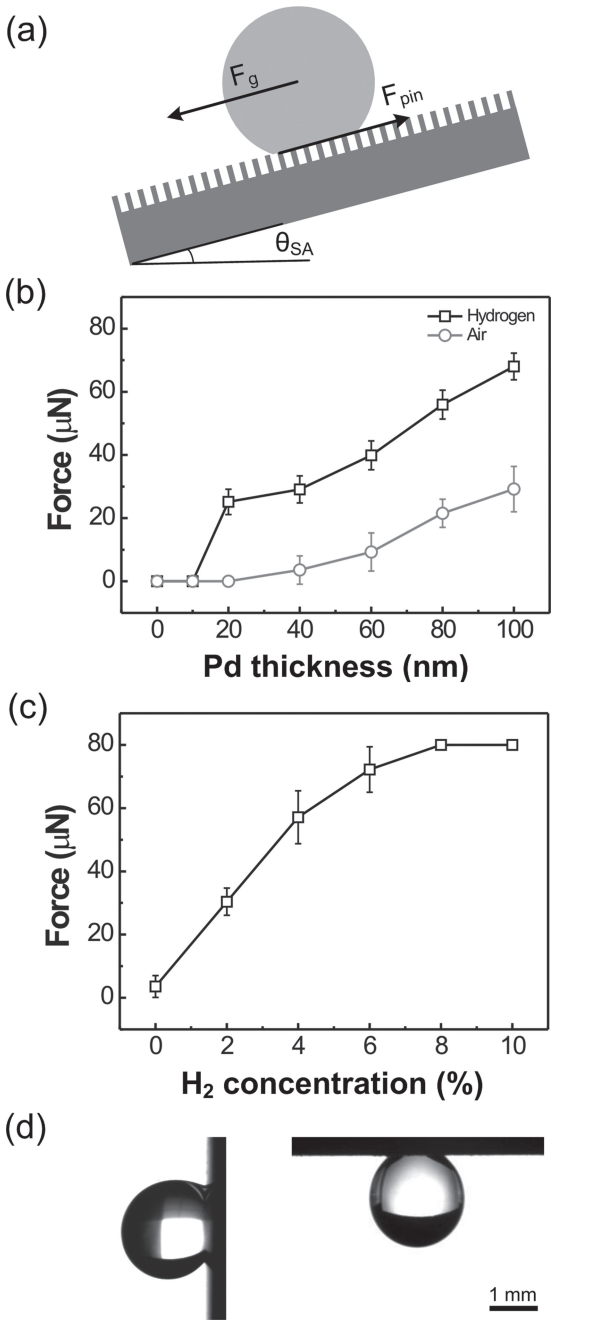

Figure 3. a) Schematic illustration of two forces that affect a water droplet on the DTS Pd/Si NW arrays when the substrate is tilted. b) Water pinning force on DTS Pd/Si NW arrays with respect to t_{Pd} under 2% H_2 and atmospheric ambient. c) Water pinning force of DTS Pd/Si NW arrays with t_{Pd} of 40 nm as a function of H_2 concentration. d) Photographs of an 8 μL of water droplet on DTS Pd/Si NW arrays at different tilt angles of 90° (left) and 180° (right) under 8% of H_2 concentration.

sliding angle (θ_{SA}), which is defined as the critical substrate tilt angle when the water droplet on DTS Pd/Si NW arrays rolled off along the direction of gravity. Macroscopically, the rolling-off of the water droplet from the surface of DTS Pd/Si NW arrays at θ_{SA} could be affected by two forces parallel to the substrate, as shown in **Figure 3**a: the gravitational force of the water droplet (F_g) and

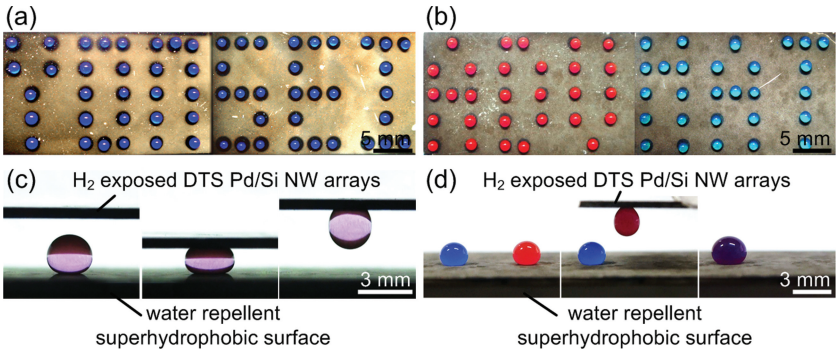

Figure 4. Photographic images of dyed water droplets which were adhered on patterned DTS Pd/Si NW arrays with t_{Pd} of 40 nm spelling: a) "YONSEI" and b) "ADV MAT", under 2% H_2 ambient. Photographs of: c) detachment of an 8 μL water droplet using the DTS Pd/Si NW arrays and d) mixing of dyed water droplets. DTS Pd/Si NW arrays with t_{Pd} of 40 nm was used for detachment and mixing of water droplets after exposure to 8% H_2 gas ambient.

the water pinning force (F_{pin}) between the water droplet and the substrate. When F_g is larger than F_{pin}, the water droplet rolls off along the direction of the gravity vector. Thus, F_{pin} could be estimated by measuring F_g at θ_{SA} using the following equation:

$$F_{pin} = -\rho V g \sin\theta_{SA}, \quad (2)$$

where ρ is the water density, V is the droplet volume, and g is the gravitational acceleration constant. In order to estimate F_{pin} with t_{pd} varying from 0 to 100 nm, we first measured θ_{SA} of an 8 μL water droplet on the DTS Pd/Si NW arrays as a function of t_{pd} under air and 2% H_2 ambient conditions. It was observed that θ_{SA} had an almost linear relationship with t_{pd} when t_{pd} was above 20 nm. θ_{SA} greatly increased when the DTS Pd/Si NW arrays were exposed to H_2, which implies that the water pinning force on the same super-hydrophobic surface of DTS Pd/Si NW arrays could be manipulated. When t_{pd} was below 10 nm, the change in super-hydrophobic adhesion properties from water-repellent to water-adhesive during the alternating ambient conditions was not observed, and the water droplet rolled off, even at a θ_{SA} of ≈0°. This can be ascribed to the insufficient contact line pinning force to hold a water droplet with a volume of 8 μL on the surface of the DTS Pd/Si NW arrays, even after the pinning force was increased by volumetric expansion of the DTS Pd/Si NW arrays under a H_2 ambient. Using 72.8 mN/m as the surface tension of water,[28] and 9.8 m/s^2 as g, F_{pin} under 2% H_2 and atmospheric ambient was estimated and plotted as a function of the deposited Pd layer thickness in Figure 3b. For t_{pd} below 10 nm, F_{pin} could not be estimated since the roll-off angle was ≈0°. In cases when $t_{pd} \geq 20$ nm, F_{pin} was substantially increased when the DTS Pd/Si NW arrays were exposed to H_2. Notably, the ratio of increase in F_{pin} was dramatically decreased with increasing t_{pd}. In contrast, F_{pin} increased by approximately >8.15 times in a H_2 ambient when t_{pd} was in the range of 20 to 50 nm, and showed a lower rate of increase (<4.2 times) when t_{pd} was above 50 nm. The large water adhesion switching contrast observed in the DTS Pd/Si NW arrays with t_{pd} between 20 and 50 nm according to different ambients could facilitate precise control of the water droplet motion on the target surface.

The super-hydrophobic adhesion force could also be affected by H_2 concentration since the phase transition of the Pd layer, which induces morphological changes of the DTS Pd/Si NW arrays, is highly dependent on H_2 concentration. Figure 3c represents the variation of the water pinning force as a function of H_2 concentration. The sliding angles and corresponding water pinning forces were measured using an 8 μL water droplet and t_{Pd} was 40 nm. Below the threshold of approximately 2% H_2, the super-hydrophobic adhesion switching was not observed, which could be ascribed to insufficient volume expansion of the Pd layer to obtain enough water adhesion force. Above 2% H_2, the water pinning force was gradually increased with H_2 concentration since the conversion percentage of Pd to PdH_x increased as the concentration of hydrogen rose. When the H_2 concentration was higher than 8%, the water sliding angle greater than 90° was achieved, indicating that the water adhesive force was large enough to firmly pin an 8 μL water droplet even when the substrate was tilted vertically (left-hand image of Figure 3d) and turned upside down (right-hand image of Figure 3d).

The water adhesive switching area could be selectively patterned using a shadow mask. **Figure 4**a,b show the selectively adhered dyed water droplets on the DTS Pd/Si NW arrays with the letter patterns, when the patterned substrate were exposed to a H_2 ambient. The concentration of H_2 was 2% and the value of t_{Pd} was 40 nm. It was observed that droplets of dyed water easily rolled off from the highly water-repellant surfaces of DTS Pd/Si NW arrays under atmospheric conditions due to the decreased surface energy by the DTS coating. When the ambient was switched to concentrated H_2, the dyed water droplets were selectively pinned on the patterned surfaces owing to the volumetric expansion of the patterned Pd layers, clearly demonstrating the letters of "YONSEI" (Figure 4a) and "ADV MAT" (Figure 4b). Not only water droplet, but various aqueous solutions such as diluted rat blood, coffee, CdSe nanoparticle suspension could be selectively pinned on the patterned DTS Pd/Si NW arrays. The pinning and rolling off of the droplets were achieved repeatedly through alternating the ambient conditions between H_2 and atmospheric. Using the gas-driven super-hydrophobic switchable DTS Pd/Si NW arrays as a water droplet tweezer, water droplets could be transferred and mixed. Figure 4c shows sequential photographs of the water droplet transfer process using the H_2 exposed DTS Pd/Si NW arrays with t_{Pd} of 40 nm. The water droplet could be successfully detached from the water repellent super-hydrophobic surface to the water adhesive DTS Pd/Si NW arrays under 8% H_2 ambient. The mixing of aqueous droplets using the water adhesion property of the DTS Pd/Si NW arrays is also feasible. Figure 4d represents a sequence of frames capturing the mixture of an 8 μL red-dyed droplet with a blue-dyed water droplet using the DTS Pd/Si NW water droplet tweezer without any water loss (see Supporting Information video for more details).

In summary, we demonstrated a facile method of obtaining a super-hydrophobic surface with ultrafast switchable water-adhesive properties by using gas-driven morphological changes of DTS Pd/Si NW arrays. By regulating the gas-ambient between

atmosphere and H_2, the super-hydrophobic adhesion of DTS Pd/Si NW arrays was repeatedly switched between water-repellent and water-adhesive. The reversible super-hydrophobic adhesion property was highly dependent on the fast adsorption and desorption of H atoms into the octahedral sites of the Pd lattice structure, which induced volumetric expansion and shrinkage of the Pd layer, thereby changing the morphologies of the DTS Pd/Si NW arrays. The capability to modulate the super-hydrophobic adhesion on a super-hydrophobic surface with a non-contact mode could be applicable to novel functional lab-on-a-chip platforms for biological and chemical based analysis.

Experimental Section

Si NW Fabrication: Vertically aligned Si NW arrays were fabricated on (100) oriented Si substrates using the AEE method.[19,29,30] A *p*-type bare Si wafer (1-10 Ω·cm) was cut into 2 cm × 2 cm samples and cleaned in a solution mixture of $NH_4OH/H_2O_2/H_2O$ (volume ratio of 1:1:5) at 65 °C for 5 minutes to remove organic contaminants. Subsequently, the native oxide was removed by immersing the samples into a 5% HF aqueous solution for 3 minutes at room temperature. The cleaned substrates were immediately dipped into an aqueous etching solution (30 mM $AgNO_3$ mixed in 4.9 M HF) at 70 °C for 30 minutes. Ag^+ ions dissolved in the solution were randomly deposited on the Si surface and formed Ag nuclei, which act like catalysts and induce a sequential oxidation and etching processes. The Si surface in contact with Ag nuclei was oxidized to become SiO_2 and the formed oxide layer was vertically etched by HF.[20] The sequential oxidation and etching processes created highly-dense etch-pits, which resulted in vertically aligned Si NW arrays. During the AEE process, undesired by-products (silver dendrites and silver nanoparticles) were generated on the top of the substrates and were removed by successive rinsing with 30 wt% HNO_3 aqueous solution and de-ionized water. The fabricated vertical arrays of Si NW arrays were dried naturally under ambient conditions.

Pd Deposition and Surface Modification of Si NW Arrays: A Pd layer was deposited on the as-fabricated Si NW arrays by DC magnetron sputter deposition under ultrahigh vacuum at 3×10^{-7} Torr. The DTS coating process was carried out by immersing the Pd/Si NW arrays in a 3 mM solution of DTS dissolved in hexane for 30 minutes at room temperature. Then, the DTS-coated substrate was cleaned with ethanol and baked at 150 °C for 1 hour to obtain a dense DTS layer. The surface morphologies of the Pd/Si NW arrays were not changed during the DTS coating process, as shown in our previous report.[30] After the DTS coating process, the wettability of Pd/Si NW arrays was drastically changed from super-hydrophilic to super-hydrophobic.

Characterization: A home-made chamber was used to characterize the super-hydrophobic adhesion properties of the vertically aligned DTS Pd/Si NW arrays by altering the gas ambient. The chamber had inlet and outlet lines for the flow of H_2 gas, and the gas flow ratio of H_2 was controlled by the equipped mass flow controller (MFC). Concentration of H_2 was controlled by its relative amount in the mixture with air while maintaining the pressure of the chamber near atmospheric pressure.

The surface morphologies of the Pd/Si NW arrays were characterized using a JEOL JSM-6360 field emission scanning electron microscope (FE-SEM) and AFM (Dimension 3100, Veeco). Water CAs were measured using ≈5 μL droplets of de-ionized water with a CA instrument equipped with a dynamic image capture camera (Phoenix 300, SEO Co., Ltd.).

Supporting Information

Supporting Information is available from the Wiley Online Library or from the author.

Acknowledgements

This research was supported in part by the Converging Research Center Program through the Ministry of Education, Science and Technology (2012K001321) and by the Priority Research Centers Program through the National Research Foundation of Korea (NRF) funded by the Ministry of Education, Science and Technology (2012-0006689). This work was also supported by National Research Foundation of Korea (NRF) grant funded by the Korean government (MEST) (No. 2011-0028594).

Received: March 4, 2013
Revised: April 9, 2013
Published online: June 4, 2013

[1] L. Feng, S. Li, Y. Li, H. Li, L. Zhang, J. Zhai, Y. Song, B. Liu, L. Jiang, D. Zhu, *Adv. Mater.* **2002**, *14*, 1857.
[2] X. Gao, L. Jiang, *Nature* **2004**, *432*, 36.
[3] M. Dickinson, *Nature* **2003**, *424*, 621.
[4] L. Feng, Y. A. Zhang, J. Xi, Y. Zhu, N. Wang, F. Xia, L. Jiang, *Langmuir* **2008**, *24*, 4114.
[5] J. A. Howarter, J. P. Youngblood, *Macromol. Rapid Commun.* **2008**, *29*, 455.
[6] L. Cao, A. K. Jones, V. K. Sikka, J. Wu, D. Gao, *Langmuir* **2009**, *25*, 12444.
[7] N. J. Shirtcliffe, G. McHale, M. I. Newton, Y. Zhang, *ACS Appl. Mater. Interfaces* **2009**, *1*, 1316.
[8] I. You, S. M. Kang, S. Lee, Y. O. Cho, J. B. Kim, S. B. Lee, Y. S. Nam, H. Lee, *Angew. Chem. Int. Ed.* **2012**, *51*, 6126.
[9] J. R. Dorvee, A. M. Derfus, S. N. Bhatia, M. J. Sailor, *Nat. Mater.* **2004**, *3*, 896.
[10] X. Feng, L. Jiang, *Adv. Mater.* **2006**, *18*, 3063.
[11] N. J. Shirtcliffe, G. McHale, M. I. Newton, C. C. Perry, F. B. Pyatt, *Appl. Phys. Lett.* **2006**, *89*, 104106.
[12] Y. Zhao, Q. H. Lu, D. S. Chen, Y. Wei, *J. Mater. Chem* **2006**, *16*, 4504.
[13] K. Uchida, N. Nishikawa, N. Izumi, S. Yamazoe, H. Mayama, Y. Kojima, S. Yokojima, S. Nakamura, K. Tsujii, M. Irie, *Angew. Chem. Int. Ed.* **2010**, *49*, 5942.
[14] M. C. Pirrung, *Angew. Chem. Int. Ed.* **2002**, *41*, 1276.
[15] D. Macbeth, S. L. Schreiber, *Science* **2000**, *289*, 5485.
[16] C. Li, R. Guo, X. Jiang, S. Hu, L. Li, X. Cao, H. Yang, Y. Song, Y. Ma, L. Jiang, *Adv. Mater.* **2009**, *21*, 4254.
[17] C. Li, Y. Zhang, J. Ju, F. Cheng, M. Liu, L. Jiang, Y. Yu, *Adv. Funct. Mater.* **2012**, *22*, 760.
[18] C. Li, F. Cheng, J.-A. Lv, Y. Zhao, M. Liu, L. Jiang, Y. Yu, *Soft Matter* **2012**, *8*, 3730.
[19] J. Seo, H. Lee, S. Lee, T. I. Lee, J.-M. Myoung, T. Lee, *Small* **2012**, *8*, 1614.
[20] C. Y. Chen, C. S. Wu, C. J. Chou, T. J. Yen, *Adv. Mater.* **2008**, *20*, 3811.
[21] A. B. D. Cassie, S. Baxter, *Trans. Faraday Soc.* **1944**, *40*, 546.
[22] F. A. Lewis, *The Palladium Hydrogen System,* Academic, New York, USA **1967**.
[23] S. T. Marshall, D. K. Schwartz, J. W. Medlin, *Sens. Actuators B: Chem.* **2009**, *136*, 315.
[24] T.-S. Wong, C.-M. Ho, *Langmuir* **2009**, *25*, 12851.
[25] C. W. Extrand, *Langmuir* **2002**, *18*, 7991.
[26] M. K. Dawood, H. Zheng, N. A. Kurniawan, K. C. Leong, Y. L. Foo, R. Rajagopalan, S. A. Khan, W. K. Choi, *Soft Matter* **2012**, *8*, 3549.
[27] C. Dorrer, J. Rühe, *Langmuir* **2007**, *23*, 3179.
[28] A. W. Adamson, A. P. Gast, *Physical Chemistry of Surfaces*, John Wiley & Sons, New York **1997**.
[29] K. Peng, A. Lu, R. Zhang, S. T. Lee, *Adv. Funct. Mater.* **2008**, *18*, 3026.
[30] J. Seo, S. Lee, J. Lee, T. Lee, *ACS Appl. Mater. Interfaces* **2011**, *3*, 4722.